CHAPTER X

Self-assembled Peptide Nanostructures for Antibacterial Applications

Y. Shi,[a] D. W. Wareham,[b, c] L. M. Phee,[b, c] and H. S. Azevedo[a]*

[a] Queen Mary, University of London, School of Engineering and Materials Science & Institute of Bioengineering, Mile End Road, London, E1 4NS, UK

[b] Queen Mary, University of London, Barts and the London School of Medicine and Dentistry & Blizard Institute, Centre for Immunobiology, London, E1 2AT, UK

[c] Barts Health NHS Trust, 80 Newark Street, London, E1 2ES, UK

*Corresponding contributor. E-mail: h.azevedo@qmul.ac.uk

Abstract

Antimicrobial resistant (AMR) bacteria are unequivocally identified as the most important global threat to human, animal and plant health in the 21st century. In humans, AMR is predicted to outstrip cancer, cardiovascular, neurological and metabolic disorders as the most important cause of death by 2050. Tackling AMR requires multidisciplinary approaches, including the repurposing and revitalization of older drugs, development of new compounds and novel strategies to deliver them for treating and preventing the spread of multi-drug resistant (MDR) bacterial infections. In this chapter, research exploiting supramolecular peptide nanotechnology for the development of antimicrobial nanomaterials is summarized, with particular emphasis on the role of molecular design and self-assembly in harnessing antimicrobial activities.

X.1 Introduction

Infections with antimicrobial resistant (AMR) bacteria have emerged as the most significant global threat to human health and the functioning of modern healthcare systems in the 21st century. The advances made in antimicrobial chemotherapy and drug design in the last century are exhausted and there are very few developmental agents in the pipeline. The problem is most acute with respect to Gram-negative bacteria, with the real threat that relatively minor infections will soon become untreatable. The World Health Organization (WHO) has repeatedly highlighted the lack of therapies for the 'ESKAPE' group of pathogens: (*Enterobacter, Staphylococcus aureus, Klebsiella, Acinetobacter, Pseudomonas aeruginosa, Enterococcus spp*) that exhibit either multi or extensive-drug resistance (M/XDR) and, in some cases, resistance to every available licensed compounds.

The potential causes for AMR are commonly subdivided into the following 5 categories: enzymatic deactivation; decreased permeability; efflux of antimicrobial, interfering with binding of target site; and adaptive alternative to inhibited process (**Figure 1**).[1] Enzymatic deactivation of antimicrobials may involve modification of the compound (e.g. aminoglycoside modifying enzymes) thereby interfering with their ability to bind with the target site,[2] or disintegration of the molecule (e.g. β-lactamases).[3, 4] Decreased permeability or uptake of an antibacterial is an effective way of excluding antimicrobials, often resulting in high level phenotypic resistance (elevated minimal inhibitory concentrations). This mechanism is usually adopted by Gram-negative bacteria, where its outer membrane already serves to exclude several classes of antimicrobials (e.g. macrolides, glycopeptides), and the passage of many antimicrobials (e.g. aminoglycosides, carbapenems) through the outer membrane hinges on the presence of compatible porin channels (water-filled channels found within the lipid bilayer membrane allowing the passage of hydrophilic molecules otherwise excluded by the hydrophobic membrane).[5] Decreased permeability may be due to reduction[6] or modification of these porins (e.g. OmpF/OmpC found in *E. coli*, OprD in *P. aeruginosa*), or change in type of porin expressed (e.g. downregulation of OmpF and upregulation of OmpC in nutrient-rich environments). Additionally, efflux pumps remove antimicrobials from the bacterial cell. A number of efflux pumps are involved in the removal

of multiple classes of compounds, conferring multi-drug resistance (e.g. AcrAB-TolC, best described in *E. coli*, expels a variety of compounds including chloramphenicol, quinolones, tetracyclines, rifampicin, fusidic acid and β-lactams).[7] AMR may also be attained by interfering with the binding of the molecule with the target site. The target site may be modified (e.g. reduction or neutralisation of charge of the lipopolysaccharide component on the Gram-negative outer membrane through mutations in PmrAB/PhoPQ/LpxACD reduces binding of polymyxins),[8-10] protected (e.g. plasmidic Qnr genes encode of DNA homologue for the fluoroquinolone target sites DNA gyrase and topoisomerase IV) or overexpressed, thereby bypassing the otherwise deleterious effect of the antimicrobial (e.g. increased production of dihydrofolate reductase and dihydropteroic acid synthase raises the concentration of trimethoprim and sulfamethaxazole required to inhibit the bacterium), resulting in resistance.[11, 12] Finally, an alternative metabolic pathway may act as a bypass route to an essential task undertaken by the bacterium, for which the antibiotic targets. For example, the action of β-lactams on peptidoglycan production in cell wall synthesis - mecA encodes for alternative penicillin-binding protein, PBP2', with reduced affinity for β-lactam antibiotics in *S. aureus* resulting in MDR strain commonly known MRSA.[13]

AMR determinants may be chromosomally encoded or acquired from mobile elements. Chromosomally encoded resistance determinants are usually passed on vertically, to daughter cells. The spread of the resistance determinants in this fashion is generally limited to clonal expansion, restricting the rate of transmission to the doubling time of host organism. This is in stark contrast to resistance encoded on mobile elements. Mobile elements (i.e. plasmids, transposons, integrons, integrated sequences) are pieces of DNA that have the ability to move from one host to another without having to undergo cell division. This is also known as horizontal transmission. Mobile elements may engage in horizontal transmission by 3 routes: transformation (uptake and integration of 'naked' DNA sequences by competent host cell), transduction (via a bacteriophage), and conjugation (cell to cell transfer of plasmids).[14]

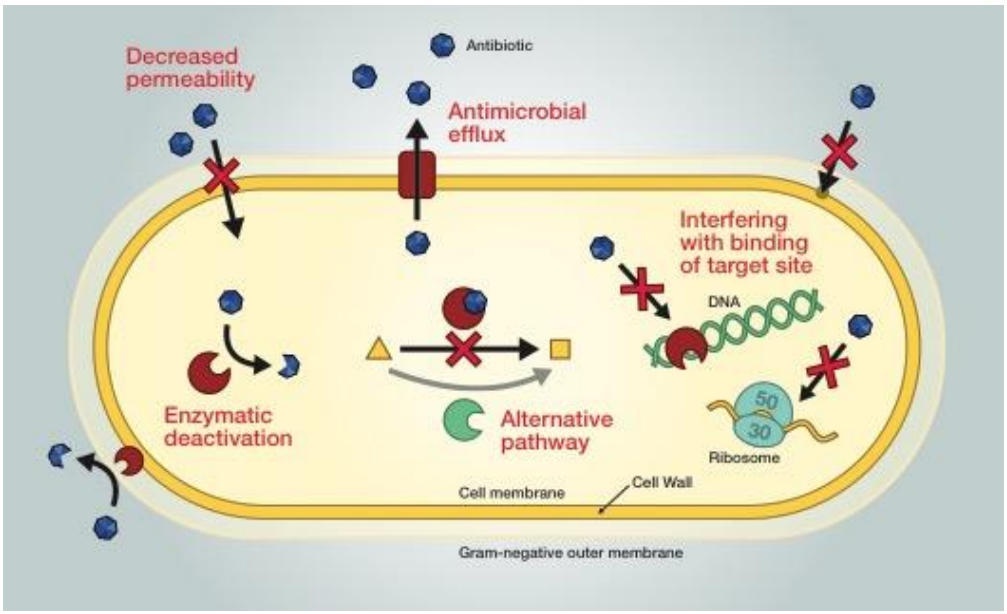

Figure 1 A general depiction of the antimicrobial resistance (AMR) mechanisms.

Solving the problem of AMR requires a translational multidisciplinary approach which will include repurposing, revitalising and refining existing agents to bridge the developmental gap and current lack of new agents. Much attention has focussed on the potential of antimicrobial peptides (AMPs), which are able to permeate and destroy the bacterial membranes, causing damage that is hard for the bacteria to fix.[15] As a consequence, it may be extremely challenging for bacteria to reconstruct their membrane systems to develop resistance to AMPs.[15] Therefore, AMR to AMPs may occurr with lower probability than that of the other availabe antibiotics. Over the past few decades, a vast number of AMPs have been isolated from different natural sources, such as virus, bacteria, as well as insects and amphibians.[16] These AMPs typically share some comon structure features. Most of them have 12-50 amino acid residues in length, carry net possitive charges, between +2 and +9, and contain around 50% hydrophobic amino acid residues.[17] The positive charge of AMPs facilitate their initial binding to the negatively charged membrane surface of bacteria through electrostatic attraction, whereas the overall amphipathic structure of AMPs allow their subsequent insertion into the hydrophobic cores of lipid bilayers and self-association and/or association with bacterial membranes.[18, 19] Despite the early success with naturally isolated AMPs as alternatives to antibiotics, their clinical applications

are limited by their high cost related to their long sequences, low stability to enzymatic degradation *in vivo*, unpredictable pharmacokinetics, and off-target cytotoxicity.[20]

To solve these inherent limitations of AMPs, emerging studies have been reported on the development of synthetic AMPs.[21] Similar to natural AMPs, these rationally designed synthetic peptides also have positve charges, as well as well-defined hydrophilic and hydrophibic moieties, which are key features for their antimicrobial activites. However, unlike many natural AMPs, synthetic peptides are relatively shorter in sequence and simpler in structure, being easier to synthesize and modify them with specific requrements, as well as being more affordable and realistic for therapeutical applications. These features also enable their use as models for further investigations to establish structure-activity relationships, revealing design rules for the development of more potent AMPs. Remarkably, due to their amphipathic structural property, some synthetic AMPs can undergo self-assembly in aqueous solution and form defined nanoscale assemblies. Upon self-assembly, physicochemical and antimicrobial properties can be boosted, such as enhanced antimicrobial activity, improved selectivity and reduced toxicity, increased proteolytic stability, as well as particular responsiveness and sustained relase.[22] The self-assembled nanostructures can be further induced to generate macroscopic materials with antibacterial properties, which can be further exploited for biomedical applications, such as wound dressing hydrogels and biomedical implants.

Herein, research on self-assembled peptide nanostructures with antimicrobial properties is summarized. Five main classes of self-assembling peptides are described, in terms of sequence design, structure characterization, self-assembly behavior and relation to antimicrobial activity. Novel peptide designs sensitive to bacterial infection conditions (enzyme, pH and bacterial surface) are also discussed, opening up the possibility for the development of more effective targeted antimicrobial therapies.

X.2 Self-Assembled Peptide Nanostructures with Antibacterial Properties

Molecular self-assembly, the spontaneous organization of molecules into ordered aggregates through non-covalent forces, have been utilized to create nanomaterials with defined structures displaying desired functionality. Peptides are excellent building blocks for self-assembly as they offer all supramolecular interactions necessary to build assemblies with controlled order. From the therapeutic point of view, peptides are also attractive as they are biocompatible and involved in many processes in human physiology, such as regulation and immune protection. AMPs have received great attention due to increasing resistance of bacteria to conventional antibiotics.[15] Some AMPs are amphipathic in nature possessing self-assembling properties and this self-assembly ability seems to correlate with their antimicrobial activity. On the other hand, some small self-assembling peptides without any bacterial killing capacity in their monomer state also seem to gain antibacterial activities upon self-assembly. Therefore, the antimicrobial activities of known self-assembling peptides have been revisited to discover new applications in antimicrobial therapies. In the following sections, five different classes of self-assembling peptides, whose assemblies were reported to display antibacterial activities, are summarized and discussed. The relationship between peptide self-assembly and their antimicrobial activity is also highlighted.

X.2.1 β-hairpin Peptides

β-hairpin is a hairpin look-like structural motif of protein. It consists of two antiparallel oriented β-strands that are connected by a short peptide loop with two to five amino acids.[23] A β-hairpin design, consisting of a 20-residue peptide and named MAX1, was proposed by Schneider and Pochan.[24] As shown in **Figure 2**, MAX1 peptide is composed of two eight-residue amphiphilic β-strands with alternating valine (V) and lysine (K) amino acids, being flanked by a tetrapeptide sequence (-V^{D}PPT-) intended to form a type II' turn structure. When dissolved in water, MAX1 peptide exhibits a random coil conformation as the peptide folding is inhibited by the repulsion force of positively charged lysine side chains. However, by raising the pH or ionic strength of the peptide solution, the side-chain charges of lysine can be effectively screened and subsequently the amphiphilic β-hairpin peptide can fold, with all hydrophobic valine residues on one face, while all

hydrophilic lysine residues on the other.[24, 25] Once folded, self-assembly of the MAX1 peptide can be driven by both hydrogen bond formation between distinct β-hairpins laterally and the hydrophobic association of the valine-rich faces of the folded peptide facially. As a result, a network of β-sheet rich fibril, which consists of bilayers of intermolecularly hydrogen bonded hairpins, self-assembles, allowing the formation of a mechanically rigid hydrogel ultimately.

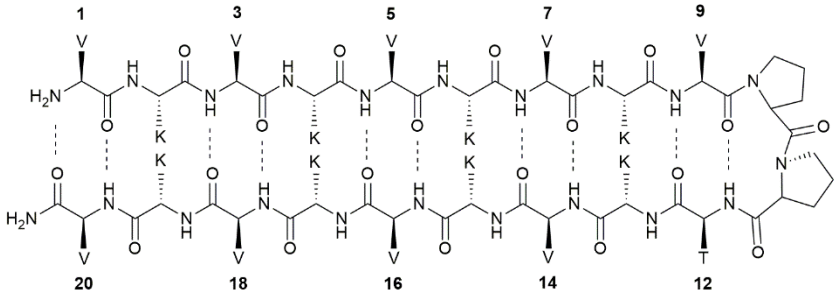

Figure 2 Sequence and proposed β-hairpin structure of MAX1 peptide.

MAX1 hydrogel was prepared by adding an equal volume of DMEM cell culture media, containing160 mM of mono- and divalent salts, directly into the aqueous peptide solution at pH 7.4. Once self-assembled, the interior of each fibril constituting the MAX1 hydrogel is hydrophobic, while the exterior is hydrophilic, displaying a large content of solvent-accessible lysine residues. Experiments demonstrated that the poly-cationic MAX1 hydrogel surfaces exhibited inherent antibacterial activity against both Gram-negative *Escherichia coli* and *Klebsiella pneumonia* bacteria, as well as Gram-positive *Staphylococcus epidermidis*, *Staphylococcus aureus*, and *Streptococcus pyogenes* bacteria.[26] By monitoring the release of β-galactosidase from cytoplasm of lactose permease-deficient *Escherichia coli* ML-35, the mechanism of the observed antibacterial activity was suggested. Upon contact with the gel surface, both the inner and outer bacterial membranes were disrupted, which led to cell death. In addition, the MAX1 hydrogel surface showed selective toxicity to bacteria versus mammalian cells, and no hemolyticity was detected towards human erythrocytes. These characteristics, together with their demonstrated potential for tissue regeneration applications, make MAX1 hydrogels excellent options as multifunctional biomaterials.

However, even though MAX1 hydrogel surface displayed ability to inhibit methicillin-susceptible *Staphylococcus aureus* (MSSA) proliferation at bacterial cell loading densities ranging from 2×10^2 to 2×10^8 CFU/dm^2, its antibacterial capacity for methicillin-resistant *Staphylococcus aureus* (MRSA) was demonstrated to be lost at higher bacterial cell loading densities (> 2×10^5 CFU/dm^2).[27] To develop an antibacterial hydrogel that is also capable of acting on drug-resistant strains, MARG1 hydrogel, with lysine residues at positions 6 and 17 of MAX1 being substituted with arginine residues (Table 1), was designed by fine-tuning the amino acid composition of the hydrophilic face of the β-hairpin.[27] Arginine is one of the mostly common amino acid present in antibacterial peptide sequences. The positively charged guanidinium headgroup of its side chain is thought to establish bidentate hydrogen bonding interactions with oxygen atoms of negatively charged macromolecules, such as lipopolysaccharide, teichoic acid, and phosphatidyl glycerol phospholipid head groups, that are displayed on the bacterial outer surfaces.[28] As expected, enhanced antibacterial action against MRSA was observed for MARG1. Even when being challenged with 2×10^8 CFU/dm^2 of bacteria, MARG1 hydrogel surface showed capability to completely inhibit the proliferation of MRSA. Additionally, MARG1 hydrogel also displayed mechanically rigid and shear stress / recovery behaviour, which allow it to be easily delivered by syringe to target sites. Further experiments proved that when the MARG1 hydrogel was syringe delivered to a lawn of MRSA that had been cultured on a nutrient-rich agar surface, bacterial cell death was observed only in the hydrogel delivered area, while no death was observed on the surrounding agar around the perimeter of the hydrogel. These results indicate that the MARG1 hydrogel can not only be applied to clean surfaces to inhibit potential infections, but can also be delivered to an infected site where bacteria can be killed upon contact.

To further investigate the importance of arginine residue on the antibacterial property of these β-hairpin hydrogels, four additional self-assembling peptides, PEP2R, PEP4R, PEP6R and PEP8R (**Table 1**), were designed and characterized.[29] In these peptides, pairs of lysine residues were replaced sequentially with arginine. Composed of the greatest number of arginine residues, PEP8R self-assembled into a hydrogel

displaying excellent antibacterial action against both *E. coli* and *S. aureus*. However, its killing effect showed no selectivity as lytic activity toward human red blood cells (hRBCs) was observed. Further cell-based assays on PEP6R, PEP4R and PEP2R revealed that decreasing the arginine content in these peptides resulted in a pronounced decrease in their haemolytic activity, while only a slight decrease in their antibacterial activity. Rheological data indicated that the arginine content of these hydrogels also influenced their mechanical rigidity. An increase in the storage modulus G' was detected with PEP6R > PEP8R > PEP4R > PEP2R. Considering the antibacterial, haemolytic and rheological properties of these hydrogels synergetically, PEP6R, that contains six arginine residues, was selected as the optimal gel. The syringe-deliverable PEP6R gel was demonstrated to have potent activity against both Gram-positive and Gram-negative bacteria, including a multi-drug resistant bacterium *P. aeruginosa*, good mesenchymal stem cell cytocompatibility, but minimal haemolyticity.

Inspired by the gelation property of these self-assembling β-hairpin peptides, bioactive peptide sequences have also been utilized as fundamental building elements to make hydrogel materials. In the work reported by Zhao's group, a gram-positive antibacterial peptide, $(KIGAKI)_3$-NH_2 was selected as a basic building block to create β-hairpin peptide for self-assembly into a hydrogel.[30] The designed β-hairpin peptide ASCP1 consists of two of this antibacterial peptide sequences, which are connected with a tetrapeptide linker (-T^{D}PPG-) serving as central loop (Table 1). When exposed to external stimuli, such as pH, ionic strength and heat, the designed ASCP1 was shown to undergo a reversible structural transition from a random coil to a stable unimolecular β-hairpin conformation, and then into an elastic hydrogel, due to the subtle balance between the electrostatic repulsion force of charged lysine residues, the hydrophobic collapse of isoleucine and alanine residues, as well as the backbone β-sheet hydrogen bonding. The self-assembled ACSP1 hydrogel was proved to have bacterial inhibitory capacity with up to 10^7 CFU/mL of *E. coli* loading.

Table 1 Summary of the application of self-assembling β-hairpin peptides for antimicrobial therapies.

Name	N-terminus	Peptide Sequences	C-terminus	Secondary Structure	Self-assembled Nanostructure	Antibacterial Activity	Cytotoxicity & Haemocytoxicity	References
MAX1	NH_2-	VKVKVKVKV^{D}PPTKVKVKVKV	-$CONH_2$	β-hairpin	β-sheet rich fibrils	active against up to 2×10^9 CFU/dm^2 *S. aureus/S. epidermidis/S. pyogenes*; 2×10^8 CFU/dm^2 *K. pneumonia*; 2×10^6 CFU/dm^2 *E. coli* initially seeded onto its surface	no toxicity on murine NIH 3T3 fibroblasts; no toxicity on hRBCs	[26, 27]
MARG1	NH_2-	VKVKVRVKV^{D}PPTKVKVRVKV	-$CONH_2$	β-hairpin	β-sheet rich fibrils	active against up to 2×10^8 CFU/dm^2 MRSA/MSSA initially seeded onto its surface	no toxicity on murine C3H10t1/2 mesenchymal stem cells	[27]
PEP8R	NH_2-	VRVRVRVRV^{D}PPTRVRVRVRV	-$CONH_2$	β-hairpin	β-sheet rich fibrils	active against 2×10^5 CFU/dm^2 *E. coli* and *S. aureus* initially seeded onto its surface	haemolyticity: ~ 25%	[29]
PEP6R	NH_2-	VKVRVRVRV^{D}PPTRVRVRVKV	-$CONH_2$	β-hairpin	β-sheet rich fibrils	active against 2×10^5 CFU/dm^2 *E. coli*, *S. aureus*, and also multi-drug resistant *P. aeruginosa* initially seeded onto its surface	minimal haemolyticity; no toxicity on murine C3H10t1/2 mesenchymal stem cells	[29]
PEP4R	NH_2-	VKVKVRVRV^{D}PPTRVRVKVKV	-$CONH_2$	β-hairpin	β-sheet rich fibrils	active against 2×10^5 CFU/dm^2 *E. coli* and *S. aureus* initially seeded onto o its surface	minimal haemolyticity	[29]
PEP2R	NH_2-	VKVKVKVRV^{D}PPTRVKVKVKV	-$CONH_2$	β-hairpin	β-sheet rich fibrils	active against 2×10^5 CFU/dm^2 *S. aureus*; less active against 2×10^5 CFU/dm^2 *E. coli* initially seeded onto its surface	minimal haemolyticity	[29]
ACSP1	NH_2-	$(KIGAKI)_3T^{D}PPG(IKAGIK)_3$	-$CONH_2$	β-hairpin	β-sheet rich fibrils	active against up to 10^7 CFU/mL *E. coli* initially seeded onto its surface	-	[30]

X.2.2 Multidomain Peptides (MDPs)

MDPs are a class of self-assembling peptides designed by Hartgerink's group. They consist of an ABA block motif, in which the B block is composed of alternating hydrophilic glutamine or serine residues and hydrophobic leucine residue, while the A block is composed of variable numbers of charges lysine or glutamate residues (**Figure 3**).[31, 32] In aqueous environment, the amphiphilic MDPs, with all hydrophilic residues lying on one face and all hydrophobic residues on the other, pack against one another into a hydrophobic sandwich due to the hydrophobic interaction. An intermolecular β-sheet hydrogen-bonding network, reinforced by hydrophobic packing, can then be assembled between two or more pairs of these sandwiches. Charged amino acids are added in both flanking A blocks to impart solubility of the formed network. Nanostructures extended from these hydrogen-bonding network reflect an energetic balance between the intermolecular hydrogen bonding and hydrophobic interactions among the hydrophilic-hydrophobic repeating units, as well as the electrostatic repulsive forces among the charges terminals. By adjusting the ratio between different blocks of MDPs, nanofibers with variable lengths can be achieved.[31] The nanofibers are assembled when the charges are screened, through the addition of oppositely charged multivalent ions, and at sufficient high concentration can entangle to form form self-supporting gels.[31, 32]

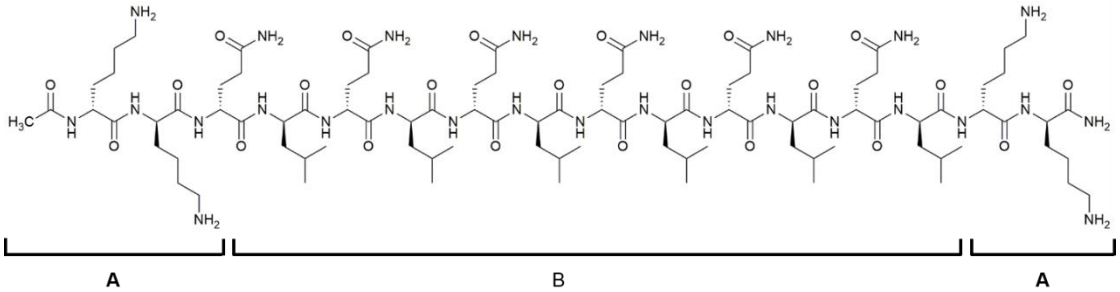

Figure 3 Sequence of a representative MDP: $K_2(QL)_6K_2$.

To systematically evaluate the cytotoxicity, protease stability and antimicrobial activity of self-assembled MDP nanostructures, Dong's group designed three MDPs: $WK_2(QL)_6K_2$, $WK_3(OL)_6K_2$ and $K_3W(QL)_6K_2$ (**Table 2**).[33] Tryptophan (W) was initially incorporated into these sequences to enable accurate concentration

measurement. However, the position of W was also found to influence the secondary structure of MDPs. Compared to $WK_3(QL)_6K_2$, the additional "KW" hydrophobic-hydrophobic repeating unit following the $(QL)_6$ domain at the *N*-terminus of $K_3W(QL)_6K_2$ increased the driving force for its β-sheet formation. Based on the circular dichroism spectra, $WK_2(QL)_6K_2$ was found to have the highest β-sheet content, followed by $K_3W(QL)_6K_2$ and $WK_3(QL)_6K_2$. Such tendency of β-sheet formation was found to correlate with the MDP nanofibers' resistance to proteolytic degradation, upon incubation with two common proteases, trypsin and chymotrypsin. The refined nanostructures are likely to prevent the access of proteases to the reaction sites through steric hindrance. Additionally, when self-assembled, the MDP nanofibers were also found to have reduced cytotoxicity toward the primary mouse bone marrow-derived monocytes (BMDMs). However, as shown in Table 2, the antimicrobial activity of these MDP nanofibers was observed to be contrary to their tendency of β-sheet formation. These results reveal that the charge density plays a minimal role in the antimicrobial activity of these MDP assemblies, since $WK_3(OL)_6K_2$ and $K_3W(QL)_6K_2$, with the same residue composition and charge density, display dramatically different antimicrobial activities. It was believed that the intermolecular interactions between MDP molecules play a key role in their self-assembly, proteolytic stability, and membrane activity that directly influences both primary cell viability and antimicrobial activity.

The same group also investigated the effect of different supramolecular nanostructures and their rheological properties on the antimicrobial activity of self-assembled MDP hydrogels by extending the 1-D soluble MDP assemblies to 3-D MDP hydrogels.[34] As shown in Table 2, the central (QL) domain of MDPs was flanked by two charged domains that comprised two or three lysine residues. Upon charge neutralization in phosphate buffer, all four MDPs, $WK_2(QL)_6K_2$, $K_2W(QL)_6K_2$, $WK_3(OL)_6K_2$ and $K_3W(QL)_6K_2$, formed hydrogels above a critical gelation concentration at 0.5 wt%. These hydrogels had storage moduli across two orders of magnitude: $K_2W(QL)_6K_2$ (~1200 Pa), followed by $WK_2(QL)_6K_2$ (~500 Pa), $K_3W(QL)_6K_2$ (~100 Pa) and $WK_3(QL)_6K_2$ (~10 Pa). The different rheological properties of these MDP hydrogels were demonstrated to be correlated with their supramolecular nanostructures observed by TEM. $K_2W(QL)_6K_2$ displayed much denser and longer nanofibers compared with the other three MDPs. Intriguingly, the different rheological properties

of these MDP hydrogels were also found to correlate with their antibacterial activities. Visual inspection of the optical images suggested that the hydrogel formed by $K_2W(QL)_6K_2$ is more efficient at inhibiting the bacterial growth, followed by $WK_2(QL)_6K_2$ and $K_3W(QL)_6K_2$. These different bactericidal activities by the MDP hydrogels were further confirmed by live/dead staining images, and quantitatively compared by bacterial colony counting assay, as well as XTT viability assay. Compared to MDP solutions, the reverse order of bactericidal activities exhibited by MDP hydrogels was postulated to be due to the formation of a large amount of elongated nanofibers, excessive charge density and porous network of the MDP hydrogel possibly trapping the bacterial cells and reducing their motility. The link between the storage modulus of the MDP hydrogels and the bacterial motility was then investigated. Through visual inspection under a confocal microscope, minimal movement of bacterial was observed in the $K_2W(QL)_6K_2$ hydrogels, which has the highest storage modulus. Moreover, these MDP hydrogels also exhibited minimum cytotoxicity to hRBCs, which lacks anionic lipids compared to bacterial cells. The exceptional bacterial cell selectivity was also explained by the susceptibility of bacteria to the formed cationic supramolecular nanofiber networks.

To further improve the hemocompatibility of these self-assembled MDP nanofibers, polyethylene glycol (PEG) with a molecular weight of 750 Da was attached to the N-terminus of MDPs (Table 2).[35] PEGylation of $WK_3(OL)_6K_2$ and $K_3W(QL)6K_2$ was found to slightly weaken their β-sheet packing, with increased helical content being detected. While the antimicrobial activity of these PEG conjugated MDPs was not compromised, as identical or even reduced MIC values were observed. It was speculated that PEG chain may not completely shield the flanking lysine residues from interacting with the negative lipid membrane to induce membrane disruption and cell death. For hemocompatibility evaluation, in addition to the most commonly used haemolysis that is easy to perform, eryptosis was also utilized to provide the full spectrum of erythrocyte injuries. Being referred to as programmed death of erythrocytes, eryptosis does not break cell membrane to the degree of causing haemolysis, thus could detect the early process of erythrocyte damage before haemolysis occurs. It was found that both MDPs exhibited dose-dependent haemolytic activity, with 10-20% haemolysis occurring at 40 μM. Upon PEGylation, dramatically decreased haemolysis was observed (~2%) because of

the stealth effect of PEG to shield cationic MDP nanofibers from disrupting the negatively charged hRBCs' membranes. However, although the two PEGylated MDPs showed comparable haemolysis rate, their eryptotic activity was significantly different, with 26% and 6% erythrocytes found to undergo phosphatidylserine externalization induced by PEG750-$WK_3(OL)_6K$ and PEG750-$K_3W(OL)_6K$, respectively. It seems that improved hemocompatibility requires PEGylation on stable MDP nanofibers with highly organized β-sheet secondary structure, while such improvement was not observed on weakly packed MDP nanofibers with partially disrupted β-sheet upon PEG conjugation. The selective hemocompatibility improvement of the MDP nanofibers upon PEG conjugation was speculated. Even PEGylation can shield the positively charged domain on MDP nanofibers from interacting with the cell membranes of hRBCs, it may also further destabilize the molecular packing of weak MDP nanofibers into individual monomers, affording them to be more flexible to dissociate and intercalate into hRBCs, which could eventually lead to enhanced eryototic activity.

To fully validate the self-assembled MDP platform for antimicrobial therapy, several fundamental questions were addressed by Dong's group.[36] The first question was whether the MDPs are assembled when in contact with lipid membranes. To answer this question, solid-state nuclear magnetic resonance (ssNMR) spectroscopy was performed on samples composed of $WK_3(QL)_6K_2$ with ^{13}C-labeled leucine residues at different sites and phospholipid liposomes. 1D cross polarization (CP) and 2D spin diffusion spectra showed that all the four ^{13}C-labelled leucine sites are in β-strand conformation. However, only the second leucine residue from the *N*-terminus formed well-defined β-strand. The local structural flexibility of the leucine residues at both *N*- and *C*- termini of the MDPs may allow accessibility of these amino acids to interact with the cell membrane. Further ^{13}C-PITHIRDs-CT spectra confirmed that MDPs interact with lipid membranes in the form of antiparallel β-sheet assemblies, rather than monomers. The MDP nanofibers and bacteria interaction was also directly visualized under TEM, showing local bacterial membrane damage induced by the MDP nanofibers. The second question was how self-assembled MDPs interact with and kill bacteria. Like most antimicrobial peptides, MDPs do not induce drug resistance in *E. coli* as the MICs of MDPs were constant after 10 passages of the bacterial culture treated with MDPs at half of its MIC value each time, while the MIC of penicillin V

was dramatically increased. Confocal laser scanning microscopy (CLSM) images demonstrated that when in presence of 20 μM $WK_3(OL)_6K_2$ for 10 min, *E. coli* could uptake rhodamine-labelled dextran (70 kDa). With extended incubation time with $WK_3(OL)_6K_2$, the bacterial cells could uptake more dextran as enhanced fluorescence was observed. More importantly, both SEM and TEM images showed the bacterial membrane disruption and hole formation when incubated with $WK_3(OL)_6K_2$. Collectively, these results provide compelling evidence about the antimicrobial mechanism of self-assembled MDP nanofibers. Upon physical contact with the bacterial membrane, the MDP nanofibers cause local membrane deformation and rupture, and eventually cell death. The third question was about the mechanism for bacterial cell selectivity of self-assembled MDPs. MDPs in their assembled state differ from their monomeric state because their hydrophobic residues are only partially exposed in the aqueous environment to interact with the hydrophobic domain of the lipid membranes. While accumulating within bacterial membranes, self-assembled MDPs were found to cross bone marrow derived monocytes (BMDMs) membranes harmlessly, allowing MDP nanofibers to possess exceptional cytocompatibility and hemocompatibility.

Building on these promising results, the MDP assemblies with intrinsic antimicrobial activity and exceptional hemocompatibility and cytocompatibility were utilized to serve as building blocks for construction of higher-ordered scaffolds that offer safer administration of therapeutic AMPs.[37] Melittin (Mel), a naturally occurring AMP with 26 residues (GIGAVLKVLTTGLPALISWIKRKRQQ) and known for its potent antimicrobial activity but severe cytotoxicity against mammalian cells, was chosen as a model therapeutic AMP to be integrated into the self-assembling MDP networks. It was conjugated to the *C*-terminus of a MDP $H_3(QL)_6$ and co-assembled with $WK_2(QL)_6K_2$. The MDPs were demonstrated to co-assemble into β-sheet nanofibers, with Mel being presented at the nanofiber surfaces. Consequently, the hydrophobic residues of Mel were found to have reduced hydrophobic interactions with the lipid membranes, leading to a considerable decrease of the Mel induced permeability of mammalian cell membranes than that of bacterial cell membranes. As a result, an increase in membrane selectivity towards bacteria was achieved. These MDP nanofibers offer unique templates for controlling the internal order and molecular packing of Mel to improve its cytocompatibility and

also hold potential for integrating multiple therapeutic AMPs with distinct sequences and structures to exert synergistic effects.

In addition to MDPs containing the sequence glutamine-leucine (QL) as their central alternating hydrophilic-hydrophobic block, a series of MDPs with serine-leucine (SL) residues in their middle domain were also reported recently having bacterial membrane-disrupting properties.[38] These MDPs with the sequence of $K_n(SL)K_n$ (n = 2, 4, 6) were reported to self-assemble into β-sheet nanofibers and form viscoelastic hydrogel networks with addition of multivalent ionic cross-linkers. The stiffness of these MDP hydrogels was found to decrease systematically with increasing terminal charge, $K_2(SL)K_2$ > $K_4(SL)K_4$ > $K_6(SL)K_6$, while the nanofibers width showed opposite trend. The storage moduli of these MDP hydrogels was also found to depend on the peptide concentration, ionic strength, and concentration of multivalent ionic cross-linker. Growth inhibition of *Pseudomonas aeruginosa* colonies was observed when these MDP hydrogels were syringe delivered into agar plates coated with bacterial films. Microsecond-time scale coarse-grained simulation was then conducted to elucidate the interaction between the MDP assemblies and bacterial membranes. The results suggested that the bacterial membrane mimic bilayer shrinks and buckles after binding to the MDP nanofibers, causing its polar head groups to become smeared and allowing water molecules to pass through the membrane. As a consequence, its core lipid tails become more disordered and the osmotic equilibrium between the intracellular and extracellular matrix of bacterial membrane is disrupted. The disruption threatens the integrity of the cellular architecture, leading to a dramatic change in the cell morphology, which has been observed and confirmed under SEM and AFM.

Table 2 Summary of the application of self-assembling multidomain peptides (MDPs) for antimicrobial therapies.

#	N-terminus	Peptide Sequences	C-terminus	CAC (μM)	Secondary Structure	Self-Assembled Nanostructure	MIC (μM)				Cytotoxicity & Hemocytoxicity	References
							E. coli	*P. aeruginosa*	*S. aureus*	*S. epidermidis*		
1	CH_3CO-	$WK_2(QL)_6K_2$	-$CONH_2$	0.87 (H_2O)	β-sheet	nanofibers	> 80	> 80	160	80	negligible cytotoxicity on BMDMs	[33, 34]
2	CH_3CO-	$K_2W(QL)_6K_2$	-$CONH_2$	-		nanofibers	-	-	> 160	-	negligible cytotoxicity on hRBCs	[34]
3	CH_3CO-	$WK_3(QL)_6K_2$	-$CONH_2$	1.24 (H_2O) 9.0 (20 mM Tris Buffer; pH 7.4)	β-sheet: 41.4 % random coils: 40% α-helix: 18.6%	nanofibers	20	20	10	5	negligible cytotoxicity on BMDMs; 10-20% haemolysis and 26.0% eryptosis at 40 μM	[33-35]
4	CH_3CO-	$K_3W(QL)_6K_2$	-$CONH_2$	1.37 (H_2O) 9.0 (20 mM Tris Buffer, pH 7.4)	β-sheet	nanofibers	80	80	20	10	negligible cytotoxicity on BMDMs; 10-20% haemolysis and 89.4% eryptosis at 40 μM	[33-35]
5	PEG750-	$WK_3(QL)_6K_2$	-$CONH_2$	8.0 (20 mM Tris Buffer, pH 7.4)	β-sheet & α-helix	short nanofibers & spherical aggregates	20	20	10	-	~2% haemolysis and 25.7% eryptosis at 40 μM	[35]
6	PEG750-	$K_3W(QL)_6K_2$	-$CONH_2$	8.5 (20 mM Tris Buffer, pH 7.4)	β-sheet & α-helix	nanofibers	80	80	10	-	~2% haemolysis and 5.58% eryptosis at 40 μM	[35]
7	CH_3CO-	$H_3(QL)_6K_2$	- Melittin (GIGAVLKV LTTGLPALI		β-sheet in Tris Buffer (20 mM, pH 7.4)	nanofibers	>80 (Mel-10%);	-	-	-	negligible cytotoxicity on NIH/3T3 fibroblasts	[37]

			SWIKRKRQQ)				10 (Mel-30%); 10 (Mel-50%)					
8	CH_3CO-	$K_n(SL)_6K_n$ (n = 2, 4, 6)	-$CONH_2$	-	β-sheet	nanofibers	-	colony-disruption ability observed	-	-	-	[38]
9	CH_3CO-	$WH_5(QL)_6K_2$	-$CONH_2$	8.6 (20 mM Tris Buffer, pH 7.4)	β-sheet at pH 7.4 α-helix & random coil at pH 5.7	-	40 acidic aerobic	-	-	-	-	[39]
10	CH_3CO-	$WH_7(QL)_6K_2$	-$CONH_2$	6.6 (20 mM Tris Buffer, pH 7.4)	β-sheet at pH 7.4 α-helix & random coil at pH 5.7	-	20 acidic aerobic	-	-	-	-	[39]
11	CH_3CO-	$WH_9(QL)_6K_2$	-$CONH_2$	9.1 (20 mM Tris Buffer, pH 7.4)	β-sheet at pH 7.4 α-helix & random coil at pH 5.7	nanofibers at pH 7.4 spherical aggregates at pH 5,7	10 anaerobic >40 aerobic	-	5 anaerobic	-	IC50 >80 µM NIH/3T3 fibroblasts HC10 >160 µM rRBCs	[39]

X.2.3 Aromatic Peptide Amphiphiles

Aromatic peptide amphiphiles have emerged as a class of simple but versatile self-assembling building blocks. They are generally composed of a short peptide segment - typically a dipeptide - with the *N*-terminus chemically capped with an aromatic moiety through a specific linker (**Figure 4**).[40] In aqueous environment, the short peptide segment and aromatic moiety of these amphiphiles work in a synergistic way for their self-assembly into diverse nanostructures, through hydrogen bonding and aromatic stacking.[41] With tailored chemical and mechanical properties, aromatic peptide amphiphile assembled nanostructures have been reported to successfully interface with biological systems for desired functions.[42, 43]

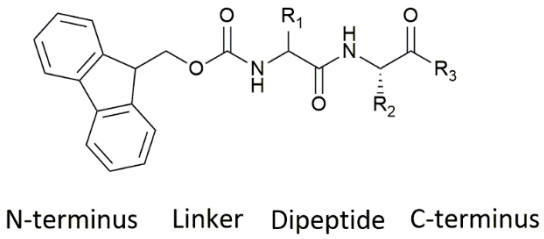

Figure 4 Chemical structure of a generic aromatic peptide amphiphile with a *N*-terminal aromatic moiety, a linker, a dipeptide segment and a C-terminus.

Diphenylalanine, the minimal self-assembling building block, was investigated by Gazit's group for its antibacterial activity towards *E. coli*.[44] The self-assembled diphenylalanine nanotubes were demonstrated to induce substantial disruption of bacterial morphology, cause bacterial outer and inner membrane permeation and depolarization, trigger upregulation of stress-response regulons, and thereby inhibit bacterial growth. Additionally, the diphenylalanine nanotubes were proved to have negligible hemotoxicity (< 2%) towards hRBCs, and also negligible cytotoxicity (< 5%) towards both HEK293 kidney cell line and HaCaT keratinocyte cell line. Further incorporation of diphenylalanine nanostructures into tissue scaffolds (agar-gelatin film) introduced antimicrobial properties into these matrices. Even though the diphenylalanine nanotubes displayed a relatively high MIC, the extensive possibilities for its chemical modifications allows

for development of diphenylalanine-based antimicrobial agents and materials with improved potency.

Conjugation of naphthalene (Nap) to the *N*-terminal of the diphenylalanine (FF) building block leads to the formation of a self-supporting gel at concentration as low as 0.4% w/v in water, due to the increased π-π interactions between aromatic groups present in the Nap and FF residues.[45] Further modification of the self-assembling NapFF with two lysine residues at its *C*-terminal endows the assembled hydrogel with significant *in vitro* antibacterial properties against the more resistant biofilm bacterial phenotype.[46] At concentration of 2% w/v, NapFFKK hydrogel was shown to reduce viable *Staphylococcus epidermidis* biofilm by 94%. However, reduction of the anti-biofilm activity has been found with the substitution of the lysine residue by ornithine, which has one less methylene unit on its *R*-group than lysine. The relatively shorter *R*-group tail was believed to make its primary amine not readily available to interact with the negatively charged bacterial membrane, thus influencing the anti-biofilm properties of the ultrashort cationic peptide hydrogel. Instead of Nap, nonsteroidal anti-inflammatory drugs, including racemic (±)-ibuprofen (Ibu), indomethacin (Ind) and (*S*)-(+)-naproxen (Npx), were attached to the *N*-terminal of FFKK peptide sequence to generate supramolecular hydrogel forming molecules, which demonstrated both antimicrobial and anti-inflammatory properties.[47] In particular, the viscoelastic hydrogel nanosponges formed by 0.4% w/v NpxFFKK displayed improved ability to target antimicrobial resistant bacterial implicated in the most severe nosocomial infections. It also improved selectivity to COX-2 implicated in chronic would scar-tissue formation.

Apart from the aromatic moieties capping, $_{D}$-amino acid conjugation at the *N*-terminal of the FF building block was also reported to generate self-assembled hydrogels in aqueous environment.[48, 49] Co-assembly of a ^{D}LFF short peptide with an aromatic antibiotic ciprofloxacin resulted in the formation of a softer gel with increased stability, compared to the gel formed by the short tripeptide alone.[50] It was postulated that ciprofloxacin molecules not only participated in intermolecular interaction with ^{D}LFF, thus reducing the ordered peptide π-stacks for softer gel formation, but also acted as bridge between the self-assembled peptide fibrils, thus providing additional branching and contact points for a more stable fibrous network. Moreover, the co-

assembled peptide hydrogel with a 30% w/w antibiotic loading, was shown to have a mild antibacterial activity against the Gram-negative *E. coli* and *K. pneumonia* bacteria by a slow release of ciprofloxacin. No major cytotoxicity was seen when culturing human red blood cells or mouse fibroblast cell on the hydrogel.

Table 3 Summary of the application of self-assembling aromatic peptides for antimicrobial therapies.

	N-terminus	Peptide Sequences	C-terminus	CAC	Secondary Structure	Self-Assembled Nanostructure	Antibacterial Activity	Cytotoxicity & Hemocytoxicity	References
1	NH_2-	FF	-COOH	0.76 mg/mL	-	unbranched nanotubes	7.1 Log reduction of *E.coli* and *L.monocytogenes* at concentration of 0.125 mg/mL; 7.3 Log reduction of *R.radiobacter* atconcentration of 0.25 mg/mL; 6.5 Log reduction of *S.epidermidis* at concentration 0.25 mg/mL	> 95% of the HEK293 kidney cells and HaCaT keratinocyte cells were viable & over 98% of the human red blood cells ramianed intact and undisrupted when treated with 250 µg/mL of FF	[44]
2	Nap-	FFKK	-COOH	-	β-sheet	nanofibers	2% w/v hydrogel significantly reduced the viable *S. epidermidis* biofilm by 94%	< 50% of the murine fibroblast (NCTC 929) were viable & significant hemolytic activity was observed upon exposure of 0.5 to 2 wt% hydrogel	[46]
3	Naproxen-(Npx-)	FFKK	-COOH	-	β-sheet	nanofibers	significant bacterial kill was observed at peptide concentrations of 1.5 wt% and above for Gram-negative *P. aeruginosa* and *E. coli*; 1.0 wt% and above for Gram-positive *S. epidermidis* and 0.5 wt% and above for *S. aureus.*	> 95% of the murine fibroblast (NCTC 929) were viable & no significant hemolysis was observed upon exposure of up to 500 µM peptide	[47]
4	Ibuprofen-(Ibu-)	FFKK	-COOH	-	β-sheet	nanoparticles	at least a three $\log_{10}$ CFU/mL reduction in *P. aeruginosa*, *E. coli*, *S. epidermidis* and *S. aureus* was observed for each NSAID-peptide at concentration of 0.5 wt% and above.		
5	Indomethacin-(Ind-)	FFKK	-COOH	-	β-sheet	nanotapes			

X.2.4 Surfactant-like Peptides (SLPs)

SLPs are a class of self-assembling peptides initially developed by Zhang's group.[51-53] These peptides typically have at least one charged amino acid (lysine, histidine, aspartic acid or glutamic acid) as their polar head and a consecutive repeat of hydrophobic amino acids (glycine, alanine, valine, leucine, or isoleucine) as their nonpolar tails (**Figure 5**). SLPs self-assemble into a variety of ordered nanostructures, such as vesicles and nanotubes, through a combination of three pivotal driving forces, the hydrophobic interaction between the hydrophobic tails, the electrostatic repulsion between charged heads and the hydrogen bonding between peptide backbones and when above a certain critical aggregation concentration in aqueous solution.

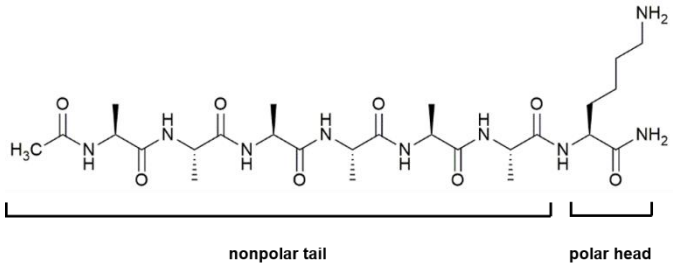

Figure 5 Chemical structure of a representative SLP: A_6K.

In the work reported by Lu and co-workers, three SLPs, A_3K, A_6K and A_9K, were designed and studied for their self-assembly behaviour. With increasing hydrophobic peptide tail regions, the nanostructures assembled from these SLPs decreased in size: from loosely packed unstable stacks for A_3K, long and stable nanofibers for A_6K, to well packed short and narrow nanorods for A_9K.[54] Further studies conducted by the same group revealed that in parallel to these morphological changes, the antibacterial activity of these SLPs exhibited a positive correlation to their hydrophobicity.[55] That is, A_9K showed the best killing capacity of all the three studied SLPs against Gram-negative *E. coli DH5α* and Gram-positive *S. aureus* bacteria. Both fluorescence assays and SEM images suggested that A_9K exerted its antibacterial activity through disrupting bacterial membranes and causing cell lysis. However, A_9K did not cause any noticeable hRBC haemolysis over the concentration range necessary for its effective bacterial killing. Upon exposure to lipid bilayers, A_9K elicit more pronounced structure perturbation on the preformed 1,2-dipalmitoyl-sn-glycero-3-phosphoglycerol

(DPPG) membrane bilayer (a bacterial membrane model) than the preformed dipalmitoyl phosphatidylcholine (DPPC) membrane bilayer (a mammalian cell membrane model). This result was entirely consistent with the high selectivity observed for the haemolytic studies, indicating high degree of selectivity for A_9K to bacterial cells than mammalian cells. Even though initial increase of the hydrophobic alanine residues enhanced the bacterial killing efficiency of the SLPs, there seems to be a threshold that brings the amphiphilic balance of these SLPs and empowers them with the optimal antibacterial capacity. Further increase of the alanine residue number to 12 made the $A_{12}K$ SLP too hydrophobic to effectively inhibit bacterial growth.[56] And addition of one more charged lysine residue to the polar head of SLP also compromised its propensity of forming β-sheet nanostructures and ability of disrupting bacterial membranes. However, A_9K_2 was shown to undergo a sol-gel transition upon addition of fetal bovine serum (FBS) or plasma amine oxidase (PAO).[57] Lysyl oxidase in FBS or PAO was proven to catalyse the lysines to allysines and attenuate the electrostatic repulsions between assembled A_9K_2 micelles and short nanorods to form aligned nanofibers, which consequently resulted in hydrogelation of A_9K_2 aqueous solution. Under coculture conditions, the A_9K_2 hydrogel displayed excellent selectivity by favouring the adherence and spreading of mammalian cells NIH 373, while killing pathogenic bacteria *B. subtilis* 168. The intrinsic antibacterial activity of A_9K_2 hydrogel endows this gel with great potential for biomedical applications while preventing bacterial contaminations.

Compared to lysine residues, arginine residues containing the guanidinium groups, were believed to have more effective membrane permeating capacity.[58] The guanidinium groups, which can delocalize the cationic charge, are able to form bidentate hydrogen bonds with the negatively charged phosphates and sulphates on the surface of cellular membranes, leading to negative curvature and hence membrane permeation. The effective membrane permeating capacity of arginine was also considered to endow the antimicrobial properties to arginine-rich AMPs. With the substitution of lysine residue with arginine, Hamley and collaborators demonstrated that A_6R peptide displayed better antibacterial activity than A_6K peptides, with a 75% - 85% CFU reduction of *E. coli* being observed when treated with 5 mg/mL of the A_6R peptides for 1 h.[59] The A_6R peptide was found to self-assemble into ultrathin sheet in aqueous solution initially, then wrap into helical

ribbons and nanotubes with increase in concentration.[60] When in contact with the preformed DPPC vesicles that mimic mammalian cell membranes, A_6R peptides did not seem to permeabilize the vesicles despite its insertion into the vesicle walls. These observations indicated that A_6R peptide could be considered as a promising antimicrobial agent with greater antimicrobial activity and without causing the lysis of mammalian cells. The same group further investigated the A_6R SLP with both its termini capped (capA_6R).[61] Compared with the uncapped A_6R, the reduced electrostatic interactions in capA_6R favoured its self-assembly into fibrils with a β-sheet structure. The capA_6R was also observed to interact preferentially with anionic model membranes (POPE/POPG) resembling those in bacteria than the zwitterionic model membrane (POPC/DOPC) resembling those in mammalian cells. These behaviours of capA_6R were in contrast with the results obtained with uncapped A_6R, which has a minimal influence on anionic membranes but could cause lamellar decorrelation of zwitterionic membranes. However, the uncapped A_6R, with weaker interactions with anionic model membrane, displayed greater antimicrobial activities against all three studied bacteria, Gram-negative *E. coli* as well as Gram-positive *S. aureus* and *L. monocytogenes*, indicating that considering the interaction of SLPs with lipid model membranes alone is insufficient to determine the antimicrobial activity. Besides, the amphiphilicity of the A_6R SLP was also altered by increasing the number of alanine residues to generate A_9R.[62] The increased hydrophobicity of the A_9R molecule favoured its self-assembly into long nanofibers with β-sheet secondary structures and hence a self-supporting hydrogel at higher concentration, even without pH adjustment. In particular, the A_9R exhibited significant selective antimicrobial activity against Gram-negative microorganisms, with a four-order of magnitude reduction in CFU/mL found for *P. aeruginosa* and a less pronounced effect in *E. coli*.

Peptide bola-amphiphiles, with charged residues at both ends of a hydrophobic amino acid sequence, belongs to another class of SLPs. Hamley's group have designed and studied the self-assembly, antimicrobial activities, and membrane interaction of a series of these peptide bola-amphiphiles: RA_3R, RA_6R and RA_9R.[63, 64] Self-assembly was only observed for RA_9R, above a critical aggregation concentration of 0.18 wt%, into β-sheet nanofibers. RA_3R and RA_6R were not found to assemble in aqueous solution, probably due to their

relatively high solubility. However, cytotoxicity studies showed that RA_3R and RA_6R were more cytocompatible than RA_9R. The high density of arginine residues presenting on the surface of RA_9R assemblies was considered to be one factor contributing to the increased cytotoxicity of RA_9R, while the increased hydrophobicity of RA_9R was also considered to play a role. Moreover, initial antimicrobial studies showed that RA_3R and RA_6R were efficient antibacterial agents against Gram-positive *L. monocytogenes* and Gram-negative *P. aeruginosa*, respectively, while RA_9R displayed little antimicrobial activity, independently of concentration. These results highlight the importance of the balance between molecular charge and hydrophobicity on the self-assembly, cytocompatibility and antimicrobial activity of peptide bola-amphiphiles. Additionally, the same group has also investigated the interactions between these peptide bola-amphiphiles and lipid bilayers with compositions related to those in bacterial and mammalian cell membranes, respectively. The results demonstrated that the peptide bola-amphiphiles have a higher affinity for lipid vesicles mimicking the bacterial cell membrane than the ones replicating the mammalian cell membrane, suggesting the ability of these peptide bola-amphiphiles to distinguish between bacterial or mammalian cells.

Table 4 Summary of the application of self-assembling surfactant-like peptides (SLPs) for antimicrobial therapies.

#	N-terminus	Peptide Sequences	C-terminus	CAC	Secondary Structure	Self-Assembled Nanostructure	Antibacterial Activity	Cytotoxicity & Hemocytoxicity	References
1	CH_3CO-	A_3K	-$CONH_2$	-	β-sheet	membrane stacks	weak bacterial killing capacity	-	[54, 55]
2	CH_3CO-	A_6K	-$CONH_2$	0.2 mM	β-sheet	nanofibers	35% and 45% CFU reductions for *E.coli* and *S. aureus*, respectively, when in contact with 0.2 mg/ml peptide for 1 h	-	[54, 55]
3	CH_3CO-	A_9K	-$CONH_2$	0.015 mM	β-sheet	nanorods	80% and 70% CFU reductions for *E.coli* and *S. aureus*, respectively, when in contact with 0.1 mg/ml peptide for 1 h	no noticeable hemolysis at concentration up to 0.1 ,g/mL; 55% haemolytic activity at concentration of 0.5 mg/mL	[54, 55]
4	CH_3CO-	$A_{12}K$	-$CONH_2$	0.005 mg/mL	β-sheet	nanorods	30% CFU reduction for *E. coli DH5α* when in contact with 0.2 mg/mL peptide for 1 h	less than 3% of human erythrocytes were lysed at concentration below 0.1 mg/mL	[56]
5	CH_3CO-	A_9K_2	-$CONH_2$	0.13 mg/mL	random coil combined with α-helix	spherical stacks and short fibers	slightly lower antibacterial ability than A_9K	less than 3% of human erythrocytes were lysed at concentration below 0.1 mg/mL	[56]
6	NH_2-	A_6R	-COOH	1.4 wt%	random coil in low concentration; β-sheet in high concentration	nanosheet (low concentration); nanorubes (high concentration)	85% - 75% CFU reduction for *E. coli* when in contact with 5 mg/mL peptide for 1 h; greater than A_6K	no membrane lysis when in contact with model DPPC vesicles mimicking mammalian cell membranes	[59, 60]

7	CH_3CO-	A_6R	-$CONH_2$	0.4 wt%	random coil (0.08-0.5 wt%); β-sheet (1 wt%)	long nanofibers	1.8, 1,2 and 4.7 log CFU reduction was observed for *E. coli*, *L. monocytogenes* and *S. aureus*, respectively when treated with 0.5 wt% of the peptides for 24 h	~ 75% viability of 161Br skin fibroblast cells when treated with peptides with a concentration up to 0.01 wt%	[61]
8	NH_2-	A_9R	-COOH	0.05 ± 0.01 wt%	β-sheet over a concentration range of 0.08-1 wt%	long nanofibers	4 orders of magnitude CFU reduction was found for *P. aeruginosa*; a less pronounced effect was found for *E. coli*; no statistically significant effect was found for *S. aureus*	~ 75% viability of 161Br skin fibroblast cells when treated with peptides with a concentration up to 0.05 wt%	[62]
9	-	RA_9R	-	0.18 ± 0.03 wt%	random coil at low concentration; β-sheet at high concentration	nanofibers	a 0.7, 2.6, 3,4 and 4.0 log CFU reduction were observed for *E.coli*, *S. aureus*, *P. aeruginosa* and *P.syringae*, respectively, with the presence of 0.1 wt% peptides for 24 h	IC_{50}: 0.025 wt% on human skin fibroblast cell line 161Br	[64]

X.2.5 Peptide Amphiphiles (PAs)

PAs are a class of self-assembling peptides developed by the Stupp group.[65] These molecules typically consist of a hydrophobic alkyl tail covalently attached to a tuneable peptide segment (**Figure 6**). In aqueous environment, the hydrophobic interactions of the alkyl tails, as well as the hydrogen bonding and electrostatic repulsions among the peptide heads, contribute in a synergic way to govern the self-assembly of PAs. Through rational design, a wide variety of nanostructures, such as fibres, ribbons, belts and micelles, were reported to form based on a delicate balance of these three driving forces.[65, 66]

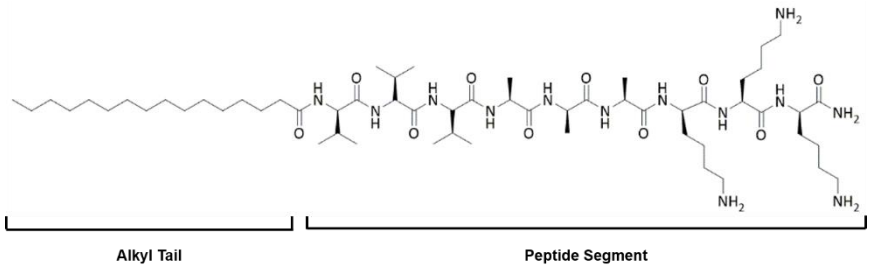

Figure 6 Chemical structure of a representative PA: $C_{15}H_{31}CONH$-VVVAAAKKK-$CONH_2$.

Palmitic acid conjugation to the *N*-terminus of variable cationic tripeptide was reported by Shai et al. to endow these nonactive short peptides with antimicrobial capacity.[67] The data obtained also suggested that the antibacterial activities and cell specificities of these PAs could be altered with the substitution of only one amino acid. For example, the C_{16}KKK PA was shown to have highly potent killing effect towards both Gram-positive and Gram-negative bacteria, as well as fungi, while C_{16}KGK PA was less active on the tested bacteria and fungi. Even worse, C_{16}KLK PA maintained only partial activity against Gram-positive bacteria and fungi, while C_{16}KAK PA seemed to completely lose the antimicrobial activity. Bacterial leakage experiments and electron microscopy visualization confirmed that all the PAs were able to induce collapse and disintegration of the microbial membranes and the order of these activities correlated with their antimicrobial capacities. Interestingly, different morphologies were observed for the PA assemblies in aqueous solution, from nanotubes for C_{16}KGK, condensed nanostacks for C_{16}KLK, to micelle-like structures for C_{16}KAK and C_{16}KKK. The organized structures may prevent PA from dissociating easily to

bound and interact with the microbial membranes, which could partially explain the differences in their antimicrobial activities.

Webster group designed an arginine-rich PA ($C_{18}GR_7RGDS$) that could self-assemble into spherical nanoparticles.[68] These nanoparticles displayed efficient ability to inhibit or delay the growth of both Gram-positive *S. aureus* and *S. epidermidis*, as well as multidrug resistant *S. aureus* (MRSA) at a low concentration range, from 2 – 20 μM, with minimal toxicity to human dermal fibroblasts. However, no killing effects were observed for Gram-negative *E. coli* and *P. aeruginosa* bacteria. The different bacteriostatic effects might be due to the existence of an outer membrane in Gram-negative bacteria, which is composed of lipopolysaccharides and proteins. The outer membrane could provide some kind of protection to the bacteria and promote different interaction modes with the positively charged spherical nanoparticles. The same group further designed a heparin-binding Cardin-motif containing PA that can self-assemble into bundle and elongated β-sheet nanofibers when above its CMC at 45 μM.[69] Antibacterial results demonstrated that the designed PA had a concentration-dependent killing effect against Gram-positive *S. aureus* and MRSA bacteria. For Gram-negative *E. coli* and MDR *E. coli* bacteria, the PA only showed effective killing effect upon self-assembly. Upon interaction with the designed PA at concentrations of 40 and 80 μM (below and above the CMC), localized bacterial membrane disintegration on Gram-positive bacteria was observed under TEM, indicating the antibacterial activity of PA on Gram-positive bacteria is independent of its self-assembly process. However, the dispersed PAs were not able to penetrate the outer membrane of Gram-negative bacteria. Only the self-assembled PAs, with increased cationic charges and β-sheet structure, were observed to insert perpendicularly into the cell wall layer of the Gram-negative bacteria and form transmembrane pores, which could initiate membrane disintegration and cytoplasmic leakage, and eventually bacteria death.

Another arginine-rich PA, which also contains the cell-penetrating peptide TAT, was designed by Yang's group.[70] Core-shell nanoparticles were reported to self-assemble and these nanoparticles were demonstrated

to have enhanced antimicrobial activities towards Gram-positive and drug-resistant Gram-positive bacteria, fungi and yeast, with low MIC values, compared to their unassembled peptide counterparts. Remarkably, with the incorporation of the cell-penetrating peptide TAT, these PA nanoparticles were shown to cross the blood-brain barrier in a *S. aureus*-induced meningitis rabbit model and inhibit the bacterial growth in the infected brain, without causing any significant toxicity to major organs. The self-assembled cationic PA nanoparticles, which were modified with TAT, were also reported by He and colleagues to penetrate the blood-brain barrier for inhibition of bacterial growth in infected brains of rats.[71] Unlike the arginine-rich PA nanoparticles reported by Yang's group, these lysine-rich PA nanoparticles showed more potent antibacterial activity against Gram-negative bacteria than Gram-positive bacteria. However, the antibacterial activities of these PA nanoparticles against Gram-positive *S. aureus* and *B. subtilis*, as well as Gram-negative *E. coli* and *P. aeruginosa*, were slightly weak when compared to the antibiotic cephalexin. Nonetheless, the killing potency of these PA nanoparticles against MRSA (MIC of 40 μM) was higher than that of cephalexin (MIC of 86 μM).

Guler and co-workers designed a self-assembling PA that contains a hydrophobic lauryl tail (C_{12}), a β-sheet forming domain (VVAG), and a short cationic antibacterial sequence (KKKGRW).[72] Upon self-assembly, the β-sheet PA nanofibers exhibited significantly enhanced antibacterial properties than the short soluble peptide (Ac-KKKGRW-Am) with random coil conformation. An eightfold improvement in the MIC value against both Gram-negative *E. coli* and Gram-positive *B. subtilis* was obtained for these nanofibers, due to the multivalent presentation of the antibacterial peptides at their periphery. Localization experiments with FITC-labelled PA demonstrated that the PA nanofibers accumulate faster on bacterial membrane than the soluble peptides. The accumulated PA nanofibers could then disrupt the bacterial membrane integrity, observed under both AFM and SEM, and was considered as the main mode for their antibacterial action.

A co-assembly system, based on a PA containing the antibacterial WMR peptide (H_2N-GIHDILKYGKPS-$CONH_2$, peptide isolated from epidermal mucus hagfish) was reported by Galdiero and collaborators.[73]

Compared to the native antibacterial WMR peptide, the WMR PA was shown to self-assemble into nanofibers, and their co-assembly with non-active PA enabled the multivalent presentation of the WMP on the surface at defined densities (Figure 7). WMR PA nanofibers were shown to significantly inhibit biofilm formation and eradicate already formed biofilms of Gram-negative *P. aeruginosa* and pathogenic fungus *C. albicans*. Moreover, the co-assembled nanostructures also exhibited low toxicity and low haemolytic activity at the concentration used for anti-biofilm assays, as well as enhanced proteolytic stability.

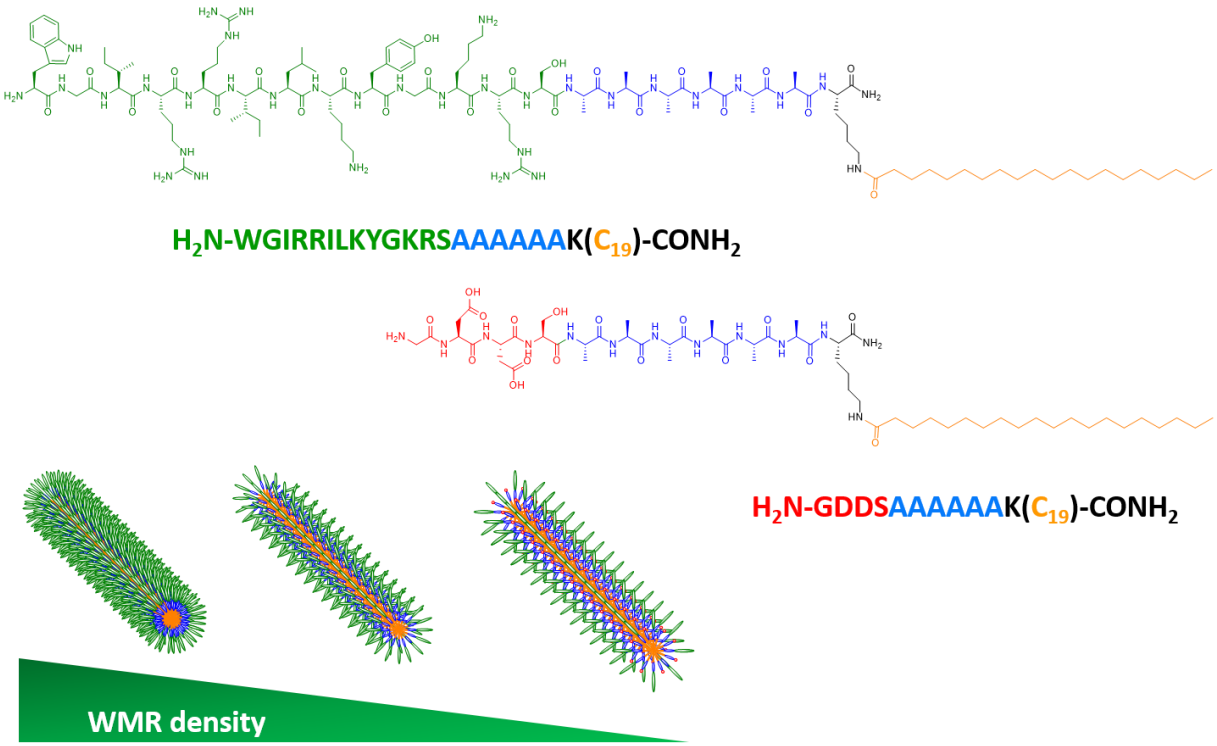

Figure 7 Chemical structures of WMR PA (top) and non-active PA (middle) and their co-assembly into nanofibers displaying different densities of WMR ligand (bottom).

Table 5 Summary of the application of self-assembling peptide amphiphiles (PAs) for antimicrobial therapies.

#	N-terminus	Peptide Sequences	C-terminus	CAC	Secondary Structure	Self-Assembled Nanostructure	Antibacterial Activity & MIC (μM)	Cytotoxicity & Hemocytoxicity	References
1	$CH_3(CH_2)_{14}CO$-	KAK	-$CONH_2$	-	-	micelles	inactive towards all tested bacteria	nonhemolytic up to 50 μM	[67]
2	$CH_3(CH_2)_{14}CO$-	KLK	-$CONH_2$	-	-	nanostacks	active against Gram-positive bacteria and fungi	nonhemolytic up to 50 μM	[67]
3	$CH_3(CH_2)_{14}CO$-	KGK	-$CONH_2$	-	-	nanotubes	active towards most bacteria and fungi	nonhemolytic up to 50 μM	[67]
4	$CH_3(CH_2)_{14}CO$-	KKK	-$CONH_2$	-	-	oligomers	highly potent towards all tested cells	onhemolytic at its MIC	[67]
5	$CH_3(CH_2)_{16}CO$-	GR_7RGDS	-COOH	-	-	spherical nanoparticles	effective to kill Gram-positive bacteria (*S. aureus, MRSA and S. epidermidis*) at a concentration range from 2-20 μM; while not effective to kill Gram-negative bacteria (*E. coli and P. aeruginosa*)	no significant toxic effect on human dermal fibroblast at concentration up to 12 μM; LC50 = 76 μM	[68]
6	$CH_3(CH_2)_{14}CO$-	$V_4K_4G(AKKARA)_2$	-COOH	45.7 μM	β-sheet in H_2O; α-helix in SDS solution	bundled and elongated nanofibers	2 log CFU reduction for Gram-positive *S. aureus* and MRSA when treated with over 80 μM peptide for 4 h; 5 log CFU reduction for Gram-negative *E. coli* when treated with over 60 μM 7peptide for 4 h and no significant reduction for *E. coli* and	minimal cytotoxicity on human dermal fibroblast at concentration from 20 to 60 μM	[69]

							MDR *E. c8oli* when treated with peptide below its CMC		
7	Cholesterol-	G_3R_6YGRKKRRQRRR	-$CONH_2$	31.6 mg/mL (10.1 μM)	-	core-shall nanoparticles	***S. aureus***: 8.1; ***methicillinresistant S. aureus***: 11.4; ***B. subtilis***: 10.7; ***E. faecalis***: 11.4; ***vancomycin-resistant Enterococcus***: 4.1; ***S. haemolyticus***: 2.0; ***C. albicans 1***: 13.0; ***C. albicans***: 10.8; ***C. tropicalis***: 13.0; ***C. neoformans***: 8.1; and ***S. chartarum***: 11.0	Relatively lower haemolytic activity on rat red blood cells than amphotericin B; no significant toxicity to major organs, such as kidney and liver after intravenous injection.	[70]
8	$CH_3(CH_2)_{10}CO$-	$WILA_2G_3K_9$YGRKKRRQRRR	-$CONH_2$	-	-	core-shall nanoparticles	***S. aureus***: 34; ***B. subtilis***: 27; ***P. aeruginosa***: 27; ***E. coli***: 27; ***methicillinresistant S. aureus***: 40	At concentration of 25 mg/L and 50 mg/L, 6% and 19% hemolysis was observed towards human red blood cells, respectively	[71]
9	$CH_3(CH_2)_{10}CO$-	VVAGKKKGRW	-$CONH_2$	-	β-sheet at pH 7.4 random coil at pH 6.5	nanofibers	***E. coli***: 125; ***B. subtilis***: 125	Negligible cytotoxicity to HUVECs	
10	NH_2-	WGIRRILKYGKRSAAAAAAK	-$CO(CH_2)_{17}CH_3$-$CONH_2$	5 μM	α-helix	short nanofibers	a loss of activity against *P. aeruginosa* biofilm, whereas an enhanced activity against *C. albicans* biofilm at 24 h when compared with its unassembled counterpart	low toxicity on Vero cells and low haemolytic activity at the concentration used for antbiofilm assays	[73]

X.3 Design of Peptide Nanostructures Responsive to Bacterial Infection Conditions

Self-assembling peptides are typically responsive to environmental stimuli. As a consequence, their physicochemical properties can change, leading for example to the release of therapeutics locally, promoting more effective treatments and reduced side effects. Although notorious success has been achieved on the application of peptide nanostructures for targeted cancer therapies, the development of stimuli-responsive peptide nanomaterials for targeted antimicrobial therapies is just getting underway. In this section, various molecular designs responsive to specific pathological conditions found at infection sites (enzyme, pH and bacterial surface) are described.

X.3.1 Enzyme

The concept of enzyme-triggered intracellular self-assembly of small peptide molecules for creating artificial nanostructures and thus controlling the fate of bacteria was firstly demonstrated by Xu's group.[74] They designed a precursor of a hydrogelator, NapFFY-($PO(OH)_2$). Once it enters *E. coli* cells by a diffusion process, the overexpressed phosphatase inside *E. coli* could convert it into a hydrogelator (NapFFY), which could then self-assemble into nanofibers and form a hydrogel. The intracellular hydrogelation was proven to change the viscosity of the cytoplasm, stress the cells, and therefore cause inhibition of growth of *E. coli*.

Based on the same concept, Ulijn's group designed and synthesized five phosphorylated precursors of aromatic dipeptides Fmoc-FY-OH, Fmoc-YT-OH, Fmoc-YS-OH, Fmoc-YN-OH and Fmoc-YQ-OH.[75] After alkaline phosphatase treatment *in vitro*, 96.0%, 97.1%, 95.0%, 99.9% and 99.9% of their precursors were converted, respectively, with Fmoc-FY-OH, Fmoc-YS-OH and Fmoc-YN-OH self-assembled into self-supporting nanofiber gels, while Fmoc-YT-OH formed clear solution containing fibrous aggregates and Fmoc-YQ-OH formed clear solution containing spherical aggregates. When cultured with *E. coli,* which was treated with inosine to over-express alkaline phosphatase, the five non-assembled precursors were shown to be converted into self-assembling aromatic peptide amphiphiles *in vivo* and increase the bacteria death to 34.9%, 28.5%, 33.1%, 46.7% and 24.9%, respectively, based on the Live/Dead cell staining assay. Even though the five

precursors exhibited similar antibacterial activities, due to their different hydrophobicity, only the more hydrophobic Fmoc-FY-OH product was found accumulated within bacterial cells, where the enzymatic conversion occurs. It was speculated that despite the dissolution and secretion from the cell, the temporary nanostructures formed intracellularly, triggered by localised concentration of self-assembled aromatic peptide amphiphiles, are sufficient to cause cell death.

X.3.2 pH

Similar to tumour tissues, some bacteria can also promote acidification of infected tissues through low oxygen triggered anaerobic fermentation. Host immune response can further lower the pH through the mechanism of lactic acid production during phagocytosis. Therefore, the acidic pH can be utilized as an environmental stimulus for the design of targeted antimicrobial therapies. Hong's group developed three self-assembling MDPs, $WH_5(QL)_6K_2$, $WH_7(QL)_6K_2$, $WH_9(QL)_6K_2$ (**Table 2**), that could undergo pH-responsive disassembly.[39] Varied numbers of histidine residues were incorporated at the *N*-terminus of MDPs to endow their pH responsiveness. At pH 5.7, which is below the p*Ka* of histidine, all the three MDPs changed from β-sheet secondary structures, displayed at pH 7.4, to weak helical/random coil conformations. By performing dialysis using a filter with Mw cut-off of 10 kDa, it was estimated that 24.60% of $WH_5(QL)_6K_2$, 34.7% of $WH_7(QL)_6K_2$, and 41.00% of $WH_9(QL)_6K_2$ were disassembled to monomers. The disassembly percentage of MDPs increased to 37.77%, 62.56% and 71.46% for $WH_5(QL)_6K_2$, $WH_7(QL)_6K_2$, $WH_9(QL)6K_2$, respectively, when using a 30 kDa filter. The pH-triggered disassembly of $WH_9(QL)6K_2$ was further confirmed by TEM, which showed a nanofiber to spherical aggregate transition with decreased pH. To visualize the disassembly of $WH_9(QL)_6K_2$ triggered by the microenvironmental pH change associated with bacterial growth, rhodamine labelled peptides (Rho-$WH_9(QL)_6K_2$) were synthesized. Reduced fluorescent intensity was observed upon self-assembly due to fluorescent quenching of Rho. In addition, using *Bacteroide fragilis* as a model bacterium and a pH ratiometric near infrared probe, a decrease in the surrounding environment from pH 7.5 to pH 6.3 was detected in less than 24 h as a result of the release of metabolites when the bacterium undergoes anaerobic growth. When Rho-$WH_9(QL)_6K_2$ was applied onto the *Bacteroide fragilis* colonies, an average of 88%

fluorescence intensity increase was observed after 24 h than that on agar without bacteria, indicating the disassembly of $WH_9(QL)_6K_2$ triggered by the local acidic pH. $WH_9(QL)_6K_2$ was further demonstrated to be effective against three bacterial strains *E. coli*, *B. fragilis*, and *S. aureus*, in the anaerobic condition where the bacterial culture gradually become acidic. $WH_9(QL)_6K_2$ was also shown to have excellent cytocompatibility toward NIH/3T3 fibroblasts (IC_{50} >80 μM), as well as hemocompatibility toward hRBCs (HC_{10} >160 μM), respectively. Taken together, the pH-triggered antimicrobial activity and excellent cytocompatibility and hemocompatibility of assembled $WH_9(QL)_6K_2$ nanofibers indicated great potential as a new strategy to effectively treat bacterial infections in which acidity plays an important role in bacterial pathogenesis.

X.3.3 Bacterial Surface

Bacterial surface-induced self-assembly of a dual fluorescent-nuclear probe for *in situ* detecting and inhibiting Gram-positive bacterial infections was also reported by Xu's group.[76] The probe, ^{125}I-Rho-FF-Van, was designed and synthesized based on modifications of both radioactive molecule indine-125 (^{125}I) and fluorescence molecule rhodamine (Rho) at the *N*-terminal of a self-assembling peptide skeleton FF, and a targeting molecule vancomyxin (Van) at the *C*-terminal. The study showed that, when Van specifically binds to the terminal peptide ($_D$-Ala-$_D$-Ala) of the methicillin-resistant *Staphylococcus aureus* (MRSA), the probe self-assembles into nanoaggregates on the MRSA surface, resulting in increased fluorescence and radioactive signals. The dual fluorescent-nuclear probe was further validated in *in vivo* myositis and pneumonia murine models, exhibiting high sensitivity and selectivity for MRSA detection.

X.4 Conclusion

Self-assembly is a facile and versatile approach to organize peptide molecules into defined nanostructures. Through rational design, distinct features could be gained by the self-assembled peptide nanostructures, such as enhanced antimicrobial activity, improved selectivity and reduced toxicity, increased proteolytic stability,

as well as tailored responsiveness and sustained release. Additionaly, self-assembled peptide nanostructures can be further exploited to create antimicrobial biomaterials, which can be implanted in different locations of the human body for treating persistent bacterial infections. Considering their synthetic simplicity and affordability, structural and functional programmability, as well as good biocompatibility and biodegradability, self-assembled peptide nanostructures show great promise not only to develop effective therapies to treat MDR bacteria infections but also to prevent bacteria growth in impant biomaterials and biomedical devices.

Acknowledgement

The authors gratefully acknowledge the Seed Award in Science (210122/Z/18/Z) granted by the Wellcome Trust.

References

1. J. M. Munita and C. A. Arias, *Microbiology spectrum*, 2016, **4**.
2. M. S. Ramirez and M. E. Tolmasky, *Drug resistance updates : reviews and commentaries in antimicrobial and anticancer chemotherapy*, 2010, **13**, 151-171.
3. E. P. Abraham and E. Chain, *Rev Infect Dis*, 1988, **10**, 677-678.
4. J. M. Frere, *Mol Microbiol*, 1995, **16**, 385-395.
5. J. M. Pages, C. E. James and M. Winterhalter, *Nature reviews. Microbiology*, 2008, **6**, 893-903.
6. D. F. Zhang, B. Jiang, Z. M. Xiang and S. Y. Wang, *Int J Antimicrob Ag*, 2008, **32**, 315-319.
7. M. N. Hall and T. J. Silhavy, *Journal of molecular biology*, 1981, **146**, 23-43.
8. L. A. Arroyo, C. M. Herrera, L. Fernandez, J. V. Hankins, M. S. Trent and R. E. W. Hancock, *Antimicrob Agents Ch*, 2011, **55**, 3743-3751.
9. A. Beceiro, A. Moreno, N. Fernandez, J. A. Vallejo, J. Aranda, B. Adler, M. Harper, J. D. Boyce and G. Bou, *Antimicrob Agents Ch*, 2014, **58**, 518-526.
10. Y. Cai, D. Chai, R. Wang, B. B. Liang and N. Bai, *J Antimicrob Chemoth*, 2012, **67**, 1607-1615.
11. J. Flensburg and O. Skold, *European journal of biochemistry*, 1987, **162**, 473-476.
12. P. Huovinen, *Clin Infect Dis*, 2001, **32**, 1608-1614.
13. C. Fuda, M. Suvorov, S. B. Vakulenko and S. Mobashery, *J Biol Chem*, 2004, **279**, 40802-40806.
14. C. M. Thomas and K. M. Nielsen, *Nature Reviews Microbiology*, 2005, **3**, 711-721.

15. M. Zasloff, *Nature*, 2002, **415**, 389-395.
16. R. E. Hancock, *Expert opinion on investigational drugs*, 2000, **9**, 1723-1729.
17. R. E. Hancock and H.-G. Sahl, *Nature biotechnology*, 2006, **24**, 1551.
18. Y. Shai, *Biopolymers*, 2002, **66**, 236-248.
19. M. R. Yeaman and N. Y. Yount, *Pharmacological reviews*, 2003, **55**, 27-55.
20. H. Jenssen, P. Hamill and R. E. Hancock, *Clinical microbiology reviews*, 2006, **19**, 491-511.
21. Z. Y. Ong, N. Wiradharma and Y. Y. Yang, *Advanced drug delivery reviews*, 2014, **78**, 28-45.
22. X. Tian, F. Sun, X. R. Zhou, S. Z. Luo and L. Chen, *Journal of peptide science : an official publication of the European Peptide Society*, 2015, **21**, 530-539.
23. B. L. Sibanda and J. M. Thornton, *Nature*, 1985, **316**, 170-174.
24. J. P. Schneider, D. J. Pochan, B. Ozbas, K. Rajagopal, L. Pakstis and J. Kretsinger, *Journal of the American Chemical Society*, 2002, **124**, 15030-15037.
25. B. Ozbas, J. Kretsinger, K. Rajagopal, J. P. Schneider and D. J. Pochan, *Macromolecules*, 2004, **37**, 7331-7337.
26. D. A. Salick, J. K. Kretsinger, D. J. Pochan and J. P. Schneider, *Journal of the American Chemical Society*, 2007, **129**, 14793-14799.
27. D. A. Salick, D. J. Pochan and J. P. Schneider, *Adv Mater*, 2009, **21**, 4120-+.
28. D. I. Chan, E. J. Prenner and H. J. Vogel, *Biochimica et biophysica acta*, 2006, **1758**, 1184-1202.
29. A. S. Veiga, C. Sinthuvanich, D. Gaspar, H. G. Franquelim, M. A. Castanho and J. P. Schneider, *Biomaterials*, 2012, **33**, 8907-8916.
30. Y. Liu, Y. Yang, C. Wang and X. Zhao, *Nanoscale*, 2013, **5**, 6413-6421.
31. H. Dong, S. E. Paramonov, L. Aulisa, E. L. Bakota and J. D. Hartgerink, *Journal of the American Chemical Society*, 2007, **129**, 12468-12472.
32. L. Aulisa, H. Dong and J. D. Hartgerink, *Biomacromolecules*, 2009, **10**, 2694-2698.
33. D. Xu, L. Jiang, A. Singh, D. Dustin, M. Yang, L. Liu, R. Lund, T. J. Sellati and H. Dong, *Chemical communications*, 2015, **51**, 1289-1292.
34. L. Jiang, D. Xu, T. J. Sellati and H. Dong, *Nanoscale*, 2015, **7**, 19160-19169.
35. D. Xu, Q. Ran, Y. Xiang, J. Linhai, B. M. Smith, F. Bou-Abdallah, R. Lund, Z. Li and H. Dong, *RSC Adv*, 2016, **6**, 15911-15919.
36. D. Xu, W. Chen, Y. J. Tobin-Miyaji, C. R. Sturge, S. Yang, B. Elmore, A. Singh, C. Pybus, D. E. Greenberg, T. J. Sellati, W. Qiang and H. Dong, *ACS infectious diseases*, 2018, **4**, 1327-1335.
37. W. Chen, S. Yang, S. Li, J. C. Lang, C. Mao, P. Kroll, L. Tang and H. Dong, *ACS applied materials & interfaces*, 2019, DOI: 10.1021/acsami.9b09583.
38. B. Sarkar, Z. Siddiqui, P. K. Nguyen, N. Dube, W. Fu, S. Park, S. Jaisinghani, R. Paul, S. D. Kozuch and D. Deng, *ACS Biomaterials Science & Engineering*, 2019, **5**, 4657-4670.
39. W. Chen, S. Li, P. Renick, S. Yang, N. Pandy, C. Boutte, K. T. Nguyen, L. Tang and H. Dong, *Journal of Materials Chemistry B*, 2019, **7**, 2915-2919.
40. S. Fleming and R. V. Ulijn, *Chemical Society reviews*, 2014, **43**, 8150-8177.
41. E. Gazit, *Prion*, 2007, **1**, 32-35.
42. D. J. Adams, *Macromolecular bioscience*, 2011, **11**, 160-173.
43. S. Marchesan, A. V. Vargiu and K. E. Styan, *Molecules*, 2015, **20**, 19775-19788.
44. L. Schnaider, S. Brahmachari, N. W. Schmidt, B. Mensa, S. Shaham-Niv, D. Bychenko, L. Adler-Abramovich, L. J. W. Shimon, S. Kolusheva, W. F. DeGrado and E. Gazit, *Nature communications*, 2017, **8**, 1365.
45. Y. Zhang, Y. Kuang, Y. Gao and B. Xu, *Langmuir*, 2011, **27**, 529-537.
46. G. Laverty, A. P. McCloskey, B. F. Gilmore, D. S. Jones, J. Zhou and B. Xu, *Biomacromolecules*, 2014, **15**, 3429-3439.
47. A. McCloskey, S. Gilmore, J. Zhou, E. Draper, S. Porter, B. Gilmore, B. Xu and G. Laverty, *RSC Advances*, 2016, **6**, 114738-114749.
48. S. Marchesan, C. D. Easton, F. Kushkaki, L. Waddington and P. G. Hartley, *Chemical communications*, 2012, **48**, 2195-2197.

49. S. Marchesan, L. Waddington, C. D. Easton, D. A. Winkler, L. Goodall, J. Forsythe and P. G. Hartley, *Nanoscale*, 2012, **4**, 6752-6760.
50. S. Marchesan, Y. Qu, L. J. Waddington, C. D. Easton, V. Glattauer, T. J. Lithgow, K. M. McLean, J. S. Forsythe and P. G. Hartley, *Biomaterials*, 2013, **34**, 3678-3687.
51. S. Vauthey, S. Santoso, H. Gong, N. Watson and S. Zhang, *Proceedings of the National Academy of Sciences of the United States of America*, 2002, **99**, 5355-5360.
52. S. Santoso, W. Hwang, H. Hartman and S. G. Zhang, *Nano Lett*, 2002, **2**, 687-691.
53. G. von Maltzahn, S. Vauthey, S. Santoso and S. U. Zhang, *Langmuir*, 2003, **19**, 4332-4337.
54. H. Xu, J. Wang, S. Han, J. Wang, D. Yu, H. Zhang, D. Xia, X. Zhao, T. A. Waigh and J. R. Lu, *Langmuir*, 2009, **25**, 4115-4123.
55. C. Chen, F. Pan, S. Zhang, J. Hu, M. Cao, J. Wang, H. Xu, X. Zhao and J. R. Lu, *Biomacromolecules*, 2010, **11**, 402-411.
56. C. Chen, J. Hu, S. Zhang, P. Zhou, X. Zhao, H. Xu, X. Zhao, M. Yaseen and J. R. Lu, *Biomaterials*, 2012, **33**, 592-603.
57. J. Bai, C. Chen, J. Wang, Y. Zhang, H. Cox, J. Zhang, Y. Wang, J. Penny, T. Waigh, J. R. Lu and H. Xu, *ACS applied materials & interfaces*, 2016, **8**, 15093-15102.
58. G. Tunnemann, G. Ter-Avetisyan, R. M. Martin, M. Stockl, A. Herrmann and M. C. Cardoso, *Journal of peptide science : an official publication of the European Peptide Society*, 2008, **14**, 469-476.
59. A. Dehsorkhi, V. Castelletto, I. W. Hamley, J. Seitsonen and J. Ruokolainen, *Langmuir*, 2013, **29**, 14246-14253.
60. I. W. Hamley, A. Dehsorkhi and V. Castelletto, *Chemical communications*, 2013, **49**, 1850-1852.
61. V. Castelletto, R. H. Barnes, K. A. Karatzas, C. J. C. Edwards-Gayle, F. Greco, I. W. Hamley, R. Rambo, J. Seitsonen and J. Ruokolainen, *Biomacromolecules*, 2018, **19**, 2782-2794.
62. V. Castelletto, C. J. C. Edwards-Gayle, I. W. Hamley, G. Barrett, J. Seitsonen and J. Ruokolainen, *ACS applied materials & interfaces*, 2019, **11**, 9893-9903.
63. V. Castelletto, R. H. Barnes, K. A. Karatzas, C. J. C. Edwards-Gayle, F. Greco, I. W. Hamley, J. Seitsonen and J. Ruokolainen, *Langmuir*, 2019, **35**, 1302-1311.
64. C. J. C. Edwards-Gayle, V. Castelletto, I. W. Hamley, G. Barrett, F. Greco, D. Hermida-Merino, R. P. Rambo, J. Seitsonen and J. Ruokolainen, *ACS applied bio materials*, 2019, **2**, 2208-2218.
65. H. Cui, M. J. Webber and S. I. Stupp, *Biopolymers*, 2010, **94**, 1-18.
66. A. C. Mendes, E. T. Baran, R. L. Reis and H. S. Azevedo, *Wires Nanomed Nanobi*, 2013, **5**, 582-612.
67. A. Makovitzki, J. Baram and Y. Shai, *Biochemistry*, 2008, **47**, 10630-10636.
68. G. Mi, D. Shi, W. Herchek and T. J. Webster, *Journal of biomedical materials research. Part A*, 2017, **105**, 1046-1054.
69. R. Chang, K. Subramanian, M. Wang and T. J. Webster, *ACS applied materials & interfaces*, 2017, **9**, 22350-22360.
70. L. Liu, K. Xu, H. Wang, P. K. Tan, W. Fan, S. S. Venkatraman, L. Li and Y. Y. Yang, *Nature nanotechnology*, 2009, **4**, 457-463.
71. B. He, S. Ma, G. Peng and D. He, *Nanomedicine : nanotechnology, biology, and medicine*, 2018, **14**, 365-372.
72. M. Beter, H. K. Kara, A. E. Topal, A. Dana, A. B. Tekinay and M. O. Guler, *Molecular pharmaceutics*, 2017, **14**, 3660-3668.
73. L. Lombardi, Y. Shi, A. Falanga, E. Galdiero, E. de Alteriis, G. Franci, I. Chourpa, H. S. Azevedo and S. Galdiero, *Biomacromolecules*, 2019, **20**, 1362-1374.
74. Z. Yang, G. Liang, Z. Guo, Z. Guo and B. Xu, *Angewandte Chemie*, 2007, **46**, 8216-8219.
75. M. Hughes, S. Debnath, C. W. Knapp and R. V. Ulijn, *Biomaterials science*, 2013, **1**, 1138-1142.
76. C. Yang, C. Ren, J. Zhou, J. Liu, Y. Zhang, F. Huang, D. Ding, B. Xu and J. Liu, *Angewandte Chemie*, 2017, **56**, 2356-2360.